Interferometric Order Parameter for Excited-State Quantum Phase Transitions in Bose-Einstein Condensates

Polina Feldmann,[1,*] Carsten Klempt,[2,3] Augusto Smerzi,[4] Luis Santos,[1] and Manuel Gessner[5]
[1]Institut für Theoretische Physik, Leibniz Universität Hannover, Appelstraße 2, 30167 Hannover, Germany
[2]Institut für Quantenoptik, Leibniz Universität Hannover, Welfengarten 1, 30167 Hannover, Germany
[3]Deutsches Zentrum für Luft- und Raumfahrt e.V. (DLR), Institut für Satellitengeodäsie und Inertialsensorik, c/o Leibniz Universität Hannover, DLR-SI, Callinstraße 36, 30167 Hannover, Germany
[4]QSTAR, INO-CNR, and LENS, Largo Enrico Fermi 2, 50125 Firenze, Italy
[5]Laboratoire Kastler Brossel, ENS-Université PSL, CNRS, Sorbonne Université, Collège de France, 24 Rue Lhomond, 75005 Paris, France

(Received 4 November 2020; revised 5 March 2021; accepted 19 April 2021; published 10 June 2021)

Excited-state quantum phase transitions extend the notion of quantum phase transitions beyond the ground state. They are characterized by closing energy gaps amid the spectrum. Identifying order parameters for excited-state quantum phase transitions poses, however, a major challenge. We introduce a topological order parameter that distinguishes excited-state phases in a large class of mean-field models and can be accessed by interferometry in current experiments with spinor Bose-Einstein condensates. Our work opens a way for the experimental characterization of excited-state quantum phases in atomic many-body systems.

DOI: 10.1103/PhysRevLett.126.230602

Quantum phase transitions (QPTs) are sudden changes in the ground-state properties of a system. The ground-state energy and wave function behave nonanalytically, and the energy gap between the ground state and the first excited state closes when, at zero temperature, a control parameter is adiabatically varied across a critical value [1]. The recently introduced excited-state quantum phase transitions (ESQPTs) [2–4] extend the concept of QPTs beyond the ground state. A particularly prominent signature of ESQPTs is given by closing gaps between excited states or, more generally, by singularities in the density of states (DOS). Typically, the critical energy is a continuous function of a control parameter. Thus, ESQPTs can be crossed both by varying a control parameter at constant energy and by varying the energy at fixed parameters.

ESQPTs have been theoretically studied in a large variety of many-body quantum systems [3,5,6], including the Lipkin-Meshkov-Glick (LMG) model [7], the Dicke and Jaynes-Cummings models [8–10], the interacting boson model [2,3,11], molecular bending transitions [12,13], and the quasienergy spectrum of driven systems [14]. Signatures of ESQPTs have been predicted, e.g., in time-averaged expectation values [15] and in the many-body dynamics after a quench [8,16,17]. However, order parameters for ESQPTs have been identified only in a very few cases [9,18,19], which limits our understanding of the excited-state phases.

Experiments on ESQPTs have so far focused on the singular behavior of the DOS in microwave Dirac billiards [20] and molecular bending transitions [21,22]. Exploring the impact of ESQPTs on the quantum many-body dynamics requires experimental platforms with flexible control over initial states and system parameters. Spinor Bose-Einstein condensates (BECs) [23,24] offer precisely such a high degree of control and provide access to the entire mean-field phase space [25]. Theoretical [23,26] and experimental [25,27,28] investigations of the mean-field dynamics of spinor BECs have revealed a separatrix characterized by diverging oscillation periods. These features are often linked to ESQPTs, suggesting spinor BECs as an exceptional platform for studies of ESQPTs. Ground-state QPTs in spinor BECs have been extensively studied [23,24,29–32]. Recently, quench dynamics revealed a dynamical QPT that has been attributed to a phase transition in the highest energy level [33,34]. In contrast, ESQPTs—i.e., phase transitions of intermediate excited states—and excited-state phases have not yet been investigated in spinor BECs.

In this Letter, we introduce an interferometrically accessible order parameter of ESQPTs in spinor BECs, which is based on the topology of mean-field phase-space trajectories. The proposed interferometric scheme distinguishes between adjacent excited-state phases and is suitable for existing experimental setups. Beyond spinor BECs, our results are relevant for a large variety of models that share the same mean-field limit. Hence, our work constitutes an important step toward the characterization of excited-state quantum phases and the systematic exploration of ESQPTs with controllable quantum many-body systems.

Ground-state quantum phases.—We consider a ferromagnetic spin-1 BEC of N atoms with three spin states $m = \pm 1,\ 0$. We assume a sufficiently weak external

trapping of the BEC such that, to a good approximation, all spin states share a common spatial mode (single-mode approximation). The spin degrees of freedom are then well described by the Hamiltonian density [23]

$$\hat{h} = \frac{q}{2N}(N - 2\hat{N}_0) + \frac{c}{N^2}\left[\hat{a}_1^\dagger \hat{a}_{-1}^\dagger \hat{a}_0^2 + \hat{a}_0^{\dagger 2}\hat{a}_1 \hat{a}_{-1} + \hat{N}_0\left(N - \hat{N}_0 + \frac{1}{2}\right) + \frac{\hat{D}^2}{2}\right], \tag{1}$$

where $\hat{a}_m^\dagger$ and $\hat{a}_m$ are the bosonic creation and annihilation operators for state m, $\hat{N}_m \equiv \hat{a}_m^\dagger \hat{a}_m$ with $\sum_m \hat{N}_m = N$, and $\hat{D} \equiv \hat{N}_1 - \hat{N}_{-1}$ is the magnetization. The interaction strength c depends on the spatial wave function and on the mass and scattering lengths of the atoms. A ferromagnetic BEC is characterized by $c < 0$ [23]. The effective quadratic Zeeman shift q incorporates microwave dressing and thus may be both positive and negative [28]. The linear Zeeman effect has been eliminated by moving to a rotating frame. The Hamiltonian density, Eq. (1), conserves $\hat{D}$ and the parity $\hat{I} = (-1)^{\hat{N}_0}$. Recently, the ground-state QPTs in the eigenspace of $\hat{D}$ with eigenvalue $D = 0$ have been both theoretically [31,35] and experimentally [36,37] investigated. Depending on the ratio $\xi \equiv q/(2|c|)$, one can distinguish the Twin-Fock (TF) phase for $\xi < -1$, the Polar (P) phase for $\xi > 1$, and the Broken-Axisymmetry (BA) phase for $|\xi| < 1$.

Excited-state quantum phases.—We focus on a ferromagnetic spin-1 BEC with zero magnetization. Strict definitions of phase transitions always refer to infinite systems. In the $N \to \infty$ limit [38–41], the spin degrees of freedom are described in terms of the classical, coherent states $|\boldsymbol{\alpha}, N\rangle \equiv (\sum_m \alpha_m \hat{a}_m^\dagger)^N |0\rangle/\sqrt{N!}$, where $\boldsymbol{\alpha} \equiv (\alpha_1, \alpha_0, \alpha_{-1})$, $\alpha_m \equiv \sqrt{n_m} e^{i\phi_m}$, $n_m \geq 0$, $\phi_m \in [0, 2\pi)$, and $\sum_m n_m = 1$. The coherent states with $\langle \hat{D} \rangle / N = n_1 - n_{-1} = 0$ yield the mean-field Hamiltonian [23,26,41]

$$\frac{h_{\mathrm{mf}}(\boldsymbol{\alpha})}{|c|} = \frac{1}{|c|} \lim_{N\to\infty} \langle \boldsymbol{\alpha}, N | \hat{h} | \boldsymbol{\alpha}, N \rangle = \xi(1 - 2n_0) - 2n_0(1 - n_0)\cos^2\phi, \tag{2}$$

where $\phi \equiv \phi_0 - (\phi_1 + \phi_{-1})/2$. Note that parity conservation results in $h_{\mathrm{mf}}(\phi + \pi) = h_{\mathrm{mf}}(\phi)$. The mean-field dynamics is governed by the equations of motion [23,26,41]

$$\frac{d}{d\tau} n_0 = \frac{\partial}{\partial \phi} \frac{h_{\mathrm{mf}}}{|c|}, \qquad \frac{d}{d\tau}\phi = -\frac{\partial}{\partial n_0}\frac{h_{\mathrm{mf}}}{|c|}, \quad \text{and} \quad \frac{d}{d\tau}(\phi_1 - \phi_{-1}) = 0 \tag{3}$$

with $\tau \equiv |c|t/\hbar$. The mean-field limit of the DOS $\nu_0(\eta)$ in the $D = 0$ subspace can be computed according to [41]

$$\lim_{N\to\infty} \frac{\nu_0(\eta)}{N} = \int \mathcal{D}\boldsymbol{\alpha}\, \delta(n_1 - n_{-1})\, \delta\left[\frac{h_{\mathrm{mf}}(\boldsymbol{\alpha})}{|c|} - \eta\right]. \tag{4}$$

Here, η denotes the energy divided by $N|c|$, $\mathcal{D}\boldsymbol{\alpha} \equiv \prod_m dn_m d\phi_m\, \delta(\sum_l n_l - 1)/(2\pi)^3$ comes from the resolution of the identity in terms of coherent states, and $\delta(n_1 - n_{-1})$ restricts the DOS to the $D = 0$ subspace. Below we employ Eqs. (3) and (4) to study signatures of ESQPTs.

Extending the ground-state phase diagram to the entire energy spectrum, we identify three excited-state phases in the ξ-η plane: the TF′ phase for $\eta > -|\xi|$ and $\xi < 0$, the P′ phase for $\eta > -|\xi|$ and $\xi > 0$, and the BA′ phase for $\eta < -|\xi|$. The phases are indicated in Fig. 1(a), where we have subtracted $\eta_0(\xi) = -\frac{1}{2}(\xi^2 + 1)$, which corresponds to the ground-state energy in the mean-field limit, from η. The excited-state phases are separated by ESQPTs at $\eta_* = -|\xi|$ with $0 < |\xi| < 1$. In the limit $|\xi| \to 0$, η_* hits the maximum of $h_{\mathrm{mf}}/|c|$. As $|\xi|$ approaches 1, the ESQPTs evolve into the known ground-state QPTs.

Signatures of ESQPTs.—As expected for ESQPTs [2,3,46], the DOS, Eq. (4), diverges at $\eta_*(\xi)$. Figure 1(a) displays the mean-field DOS as a function of ξ and $\eta - \eta_0$. Furthermore, it shows that in a finite-size system the ESQPTs reveal themselves by a sequence of avoided crossings in the energy spectrum [2]. The divergence of the DOS is due to stationary points of h_{mf}. At a stationary point, $\partial_\phi h_{\mathrm{mf}} = \partial_{n_0} h_{\mathrm{mf}} = 0$ causes the integrand in Eq. (4) to become singular. There are three stationary points at each $0 < |\xi| < 1$: a saddle point at η_* and two minima at η_0. The saddle point is located at $n_0 = 0$ for $\xi < 0$ or at $n_0 = 1$ for $\xi > 0$, and the minima are at $n_0 = (\xi + 1)/2$ and $\cos^2(\phi) = 1$ [see Fig. 1(b)]. Note that these stationary points do not depend on the restriction to coherent states with $\langle \hat{D} \rangle = 0$, which further justifies our focus on zero magnetization.

The phase-space trajectories [41] of h_{mf} provide further signatures of the ESQPTs. The classical phase space is a sphere with z coordinate n_0 and azimuthal angle ϕ. Figure 1(b) shows exemplary trajectories for $\xi = 0.5$. The trajectories reflect the symmetry $h_{\mathrm{mf}}(\phi + \pi) = h_{\mathrm{mf}}(\phi)$. Since $h_{\mathrm{mf}}(\xi, n_0, \phi) = h_{\mathrm{mf}}(-\xi, 1 - n_0, \phi)$, for $\xi < 0$ the phase space would appear upside down. As in the LMG model [47], the sets of trajectories at fixed ξ and η (the energy hypersurfaces) change topology at $\eta_*(\xi)$—at the critical energy hypersurfaces called separatrices. For $\eta > \eta_*$, i.e., in the TF′ and P′ phases, there is only one trajectory per ξ and η. By contrast, for $\eta < \eta_*$, i.e., in the BA′ phase, the evolution can follow one of two disconnected trajectories. Each of these trajectories breaks the classical symmetry $h_{\mathrm{mf}}(\phi + \pi) = h_{\mathrm{mf}}(\phi)$. Note, however, that the corresponding quantum symmetry I cannot be broken in the $D = 0$ subspace, where all states belong to a single eigenspace of I.

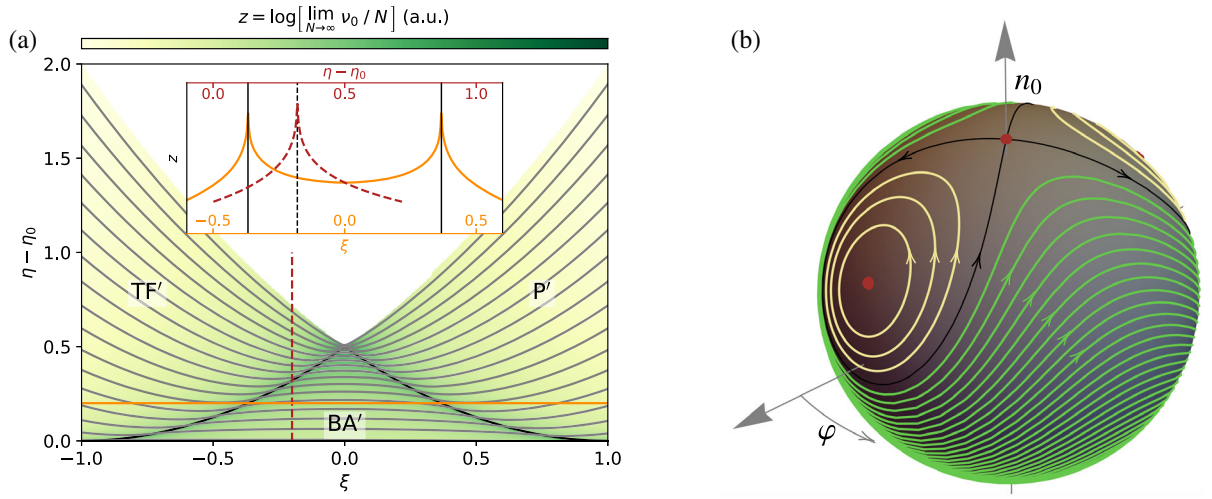

FIG. 1. Excited-state quantum phases of a ferromagnetic spin-1 BEC with zero magnetization. (a) DOS in the mean-field limit as a function of ξ and $\eta - \eta_0$ with $\eta_0(\xi) = -\frac{1}{2}(\xi^2 + 1)$. The ESQPTs at $\eta_* = -|\xi|$ (black) divide the ξ-η plane into three phases: the TF′ phase, the P′ phase, and the BA′ phase. The DOS diverges at the ESQPTs. The inset shows the DOS along lines of constant $\xi = -0.2$ (red, dashed) and $\eta - \eta_0 = 0.2$ (orange, solid). The spectrum of a BEC of $N = 100$ atoms (gray, every third eigenvalue) exhibits avoided crossings at the ESQPTs. (b) Classical phase space and trajectories for $\xi = 0.5$. The separatrix (black) separates trajectories in the P′ phase ($\eta > \eta_*$, green) with winding number $w = 1$ from trajectories in the BA′ phase ($\eta < \eta_*$, yellow) with $w = 0$. Stationary points of h_{mf} are marked in red.

Order parameter.—All solutions $n_0(t)$ and $\phi(t)$ of the classical equations of motion, Eq. (3), that do not have minimal, maximal, or critical energy density are periodic [23,26,41]. In the TF′ and P′ phases, the phase-space trajectories encircle the n_0 axis [green curves in Fig. 1(b)]—clockwise in the TF′ phase and counterclockwise in the P′ phase. By contrast, the trajectories in the BA′ phase do not enclose the n_0 axis (yellow curves). We define our order parameter w as the winding number of the classical trajectories with respect to the n_0 axis such that $w = -1$ in the TF′, $w = 1$ in the P′, and $w = 0$ in the BA′ phase. We observe that w can be expressed in a particularly simple form. Let us denote the period of $n_0(t)$ at fixed ξ and η by T. In the BA′ phase, the periods of $\phi(t)$ and $n_0(t)$ coincide and, thus, $\phi(t + T) = \phi(t)$. In the TF′ and P′ phases, however, $\phi(t + T) = \phi(t) \pm \pi$. Hence,

$$w = \frac{1}{\pi}[\phi(T) - \phi(0)]. \tag{5}$$

The winding number w is an order parameter that qualitatively distinguishes the excited-state phases by the dynamics of coherent states. It is defined for all energy densities except for the lowest, highest, and critical ones.

In the following, we present an interferometric scheme that extracts $p \equiv \cos(\pi w)$ and therefore distinguishes between neighboring excited-state phases. To measure p, first, an initial point $(n_0(0), \phi(0))$ on a trajectory at the ξ and η of interest is selected. Then the corresponding coherent state with $\phi_1 = \phi_{-1}$, $|\psi(0)\rangle$, is prepared at $q = 2|c|\xi$. The state freely evolves for the time T. Next, the spin states $m = 0$ and $m = \pm 1$ are coupled by the internal-state beam splitter $\exp[-i(\pi/2)\hat{S}_{\tilde{\theta}}]$ with $\hat{S}_\theta \equiv \frac{1}{2}(e^{-i\theta}\hat{a}_0^\dagger \hat{g} + e^{i\theta}\hat{g}^\dagger \hat{a}_0)$, $\hat{g} \equiv (\hat{a}_1 + \hat{a}_{-1})/\sqrt{2}$, and $\tilde{\theta} \equiv \pi/2 - \phi(0)$. Finally, the expectation value of $\hat{N}_0/N$ is measured. In the mean-field limit, this yields [41]

$$\lim_{N\to\infty} \frac{1}{N} \langle \psi(T)| e^{i(\pi/2)\hat{S}_{\tilde{\theta}}} \hat{N}_0 e^{-i(\pi/2)\hat{S}_{\tilde{\theta}}} |\psi(T)\rangle = \frac{1 - Vp}{2}, \tag{6}$$

where we have introduced the visibility $V = 2\sqrt{1 - n_0(0)}\sqrt{n_0(0)}$.

Experimental realization.—We detail the measurement of p for ^{87}Rb atoms in their hyperfine ground state [32,48]. However, most of our discussion applies to any ferromagnetic spin-1 BEC. We assume that, initially, the condensate is in the state $\hat{a}_0^{\dagger N}|0\rangle/\sqrt{N!}$. Then a coherent state characterized by $n_0(0)$, $\phi(0)$, and $\phi_1 = \phi_{-1}$ can be obtained by applying $\exp(-i\chi\hat{S}_{\tilde{\theta}})$ with $\cos^2(\chi/2) = n_0(0)$. Thus, both the state preparation and the beam splitter are generated by $\hat{S}_{\tilde{\theta}}$ and can be implemented by a sequence of a detuned 2π microwave pulse yielding the phase shift $\exp(i\tilde{\theta}\hat{N}_0)$, a radio-frequency pulse $\exp(-i\zeta\hat{S}_0)$ with $\zeta = \chi$ or $\zeta = \pi/2$, respectively, and another microwave pulse $\exp(-i\tilde{\theta}\hat{N}_0)$ [49,50]. Since we aim at the expectation value in Eq. (6), the first step of the state preparation and the last one of the beam splitter can be omitted. N_0 can be measured, e.g., by applying a magnetic-field gradient that spatially separates the different spin states and subsequent absorptive imaging.

Reliably distinguishing $p = \pm 1$ requires a large visibility V, which can be maximized by choosing $n_0(0)$ as close to $1/2$ as possible. The optimal $n_0(0)$, n_{opt}, is [41]

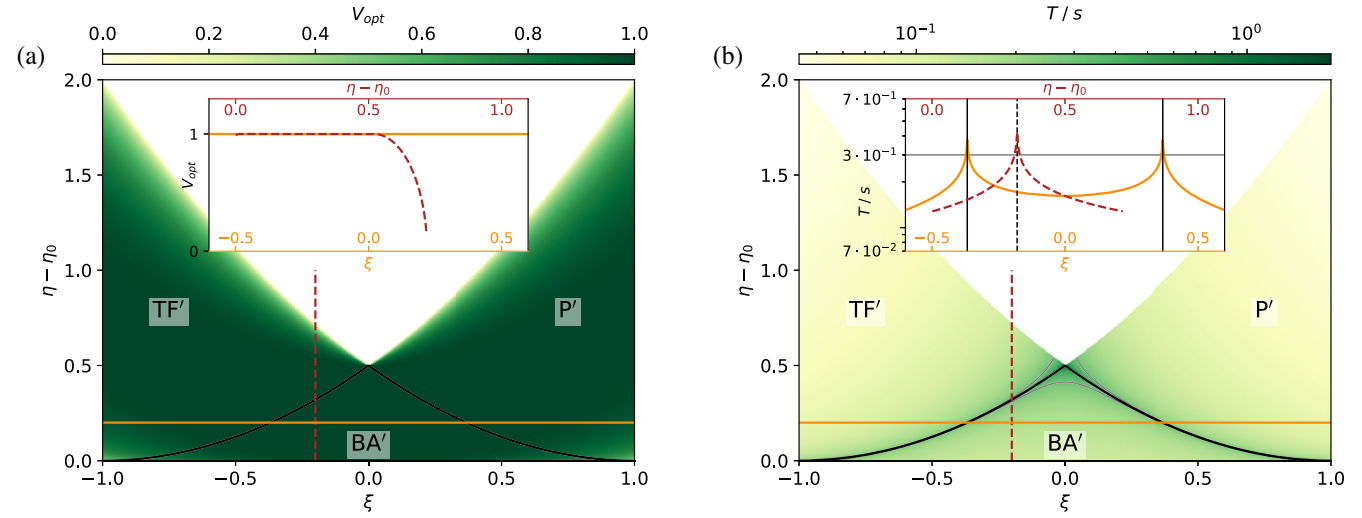

FIG. 2. Measuring $p = \cos(\pi w)$ to distinguish adjacent excited-state quantum phases requires a large optimal visibility V_{opt} and a short periodicity T. (a) V_{opt} is large throughout the vast majority of the phase diagram. (b) T for $|c|/\hbar = 2\pi \times 4$ Hz. A moderate value of 0.3 s (gray) is surpassed only at the immediate vicinity of the ESQPTs. (a), (b) Black lines mark the ESQPTs. The insets show V_{opt} and T along lines of constant $\xi = -0.2$ (red, dashed) and $\eta - \eta_0 = 0.2$ (orange, solid).

$$n_{\mathrm{opt}} = \begin{cases} \frac{1}{2}\left(1 + \xi - \frac{\xi}{|\xi|}\sqrt{1 + 2\eta + \xi^2}\right) & \text{for } \eta < -\frac{1}{2} \\ \frac{1}{2} & \text{for } -\frac{1}{2} \le \eta \le 0 \\ \frac{1}{2}\left(1 - \frac{\eta}{\xi}\right) & \text{for } 0 < \eta \end{cases} \tag{7}$$

A corresponding $\phi(0)$, ϕ_{opt}, is obtained from

$$\cos^2 \phi_{\mathrm{opt}} = \frac{\xi(1 - 2n_{\mathrm{opt}}) - \eta}{2n_{\mathrm{opt}}(1 - n_{\mathrm{opt}})}. \tag{8}$$

Figure 2(a) shows that the optimized visibility is large throughout the vast majority of the phase diagram.

The coherence time in typical BEC experiments is limited to a few seconds. This constrains the accessible periods T. It is known [23,26,41] that

$$\frac{|c|}{\hbar} T = \begin{cases} y^{-1/2} K(x/y) & \text{for } \eta < \eta_* \\ x^{-1/2} K(y/x) & \text{for } \eta > \eta_* \end{cases}, \tag{9}$$

where $K(k^2) = \int_0^{\pi/2} d\gamma (1 - k^2 \sin^2\gamma)^{-1/2}$ is the complete elliptic integral of the first kind, $x = |\xi|\sqrt{1 + \xi^2 + 2\eta}$, and $y = (x - \xi^2 - \eta)/2$. T diverges at the ESQPTs. Figure 2(b) displays T for the typical interaction strength $|c|/\hbar = 2\pi \times 4$ Hz. Fortunately, T exceeds a moderate value of, e.g., 0.3 s only in the immediate vicinity of the ESQPTs.

So far we have considered only the mean-field limit $N \to \infty$. To study the impact of a finite system size, we simulate a measurement of p for $N = 100$ bosons by exact diagonalization of the Hamiltonian density (1) (see Fig. 3). The jump discontinuities signaling the ESQPTs in the mean-field limit are, as expected, smoothed at finite N. However, the BA′ phase can still be clearly distinguished from the TF′ and P′ phases. In typical experiments, N is of the order of 10^4 and, thus, a much further convergence to the mean-field limit can be expected.

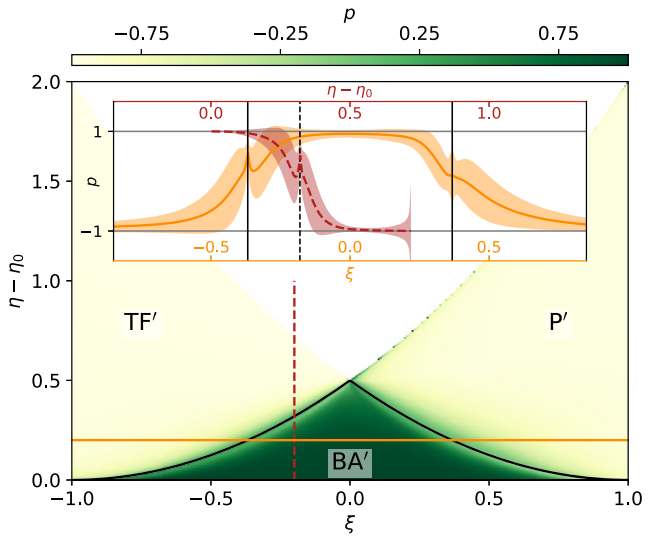

FIG. 3. Simulated measurement of p for $N = 100$ atoms. The finite-size results closely resemble the mean-field limit, where $p = 1$ in the BA′ phase and $p = -1$ in the TF′ and P′ phases. Black lines mark the ESQPTs. The inset shows p along lines of constant $\xi = -0.2$ (red, dashed) and $\eta - \eta_0 = 0.2$ (orange, solid). The shaded regions indicate the standard deviation.

Conclusions.—We have shown that ESQPTs in spinor BECs can be characterized by an interferometrically accessible order parameter, which distinguishes the excited-state quantum phases by the topology of mean-field trajectories. Unlike in the Tavis-Cummings model [9], the local order parameter $\hat{N}_0/N$ that characterizes the relevant ground-state QPTs in spinor BECs [31,32] cannot be directly generalized to excited states. Moreover, in contrast to order parameters based on long-term quench dynamics [18,19], our approach does not depend on a quantum symmetry breaking at the ESQPT.

Our findings apply to any of the numerous quantum systems with the same mean-field limit, including bosonic two-level pairing models at zero generalized angular momentum [3]. Our theoretical treatment of ESQPTs complements previous studies for the opposite sign of interaction [3]. Bosonic two-level pairing models comprise, e.g., the LMG model, the vibron model for molecules, and the interacting boson model for nuclei.

We thank Dmytro Bondarenko, Pavel Cejnar, Ignacio Cirac, and Reinhard Werner for valuable discussions. We acknowledge support by the Deutsche Forschungsgemeinschaft (DFG, German Research Foundation) under the SFB 1227 "DQ-mat", project A02, and under Germany's Excellence Strategy—EXC-2123 QuantumFrontiers—390837967, and by the LabEx ENS-ICFP: ANR-10-LABX-0010/ANR-10-IDEX-0001-02 PSL*.

*polina.feldmann@itp.uni-hannover.de

[1] S. Sachdev, *Quantum Phase Transitions*, 2nd ed. (Cambridge University Press, Cambridge, England, 2011), https://dx.doi.org/10.1017/CBO9780511973765.
[2] P. Cejnar, M. Macek, S. Heinze, J. Jolie, and J. Dobeš, Monodromy and excited-state quantum phase transitions in integrable systems: Collective vibrations of nuclei, J. Phys. A **39**, L515 (2006).
[3] M. A. Caprio, P. Cejnar, and F. Iachello, Excited state quantum phase transitions in many-body systems, Ann. Phys. (Amsterdam) **323**, 1106 (2008).
[4] P. Cejnar, P. Stránský, M. Macek, and M. Kloc, Excited-state quantum phase transitions, J. Phys. A **54**, 133001 (2021).
[5] P. Stránský, M. Macek, and P. Cejnar, Excited-state quantum phase transitions in systems with two degrees of freedom: Level density, level dynamics, thermal properties, Ann. Phys. (Amsterdam) **345**, 73 (2014).
[6] P. Stránský, M. Macek, A. Leviatan, and P. Cejnar, Excited-state quantum phase transitions in systems with two degrees of freedom: II. Finite-size effects, Ann. Phys. (Amsterdam) **356**, 57 (2015).
[7] F. Leyvraz and W. D. Heiss, Large-n Scaling Behavior of the Lipkin-Meshkov-Glick Model, Phys. Rev. Lett. **95**, 050402 (2005).
[8] P. Pérez-Fernández, P. Cejnar, J. M. Arias, J. Dukelsky, J. E. García-Ramos, and A. Relaño, Quantum quench influenced by an excited-state phase transition, Phys. Rev. A **83**, 033802 (2011).
[9] T. Brandes, Excited-state quantum phase transitions in Dicke superradiance models, Phys. Rev. E **88**, 032133 (2013).
[10] M. A. Bastarrachea-Magnani, S. Lerma-Hernández, and J. G. Hirsch, Comparative quantum and semiclassical analysis of atom-field systems. I. Density of states and excited-state quantum phase transitions, Phys. Rev. A **89**, 032101 (2014).
[11] M. Macek, P. Stránský, A. Leviatan, and P. Cejnar, Excited-state quantum phase transitions in systems with two degrees of freedom. III. Interacting boson systems, Phys. Rev. C **99**, 064323 (2019).
[12] F. Pérez-Bernal and F. Iachello, Algebraic approach to two-dimensional systems: Shape phase transitions, monodromy, and thermodynamic quantities, Phys. Rev. A **77**, 032115 (2008).
[13] D. Larese and F. Iachello, A study of quantum phase transitions and quantum monodromy in the bending motion of non-rigid molecules, J. Mol. Struct. **1006**, 611 (2011).
[14] V. M. Bastidas, P. Pérez-Fernández, M. Vogl, and T. Brandes, Quantum Criticality and Dynamical Instability in the Kicked-Top Model, Phys. Rev. Lett. **112**, 140408 (2014).
[15] G. Engelhardt, V. M. Bastidas, W. Kopylov, and T. Brandes, Excited-state quantum phase transitions and periodic dynamics, Phys. Rev. A **91**, 013631 (2015).
[16] L. F. Santos and F. Pérez-Bernal, Structure of eigenstates and quench dynamics at an excited-state quantum phase transition, Phys. Rev. A **92**, 050101(R) (2015).
[17] M. Kloc, P. Stránský, and P. Cejnar, Quantum quench dynamics in Dicke superradiance models, Phys. Rev. A **98**, 013836 (2018).
[18] R. Puebla, A. Relaño, and J. Retamosa, Excited-state phase transition leading to symmetry-breaking steady states in the Dicke model, Phys. Rev. A **87**, 023819 (2013).
[19] R. Puebla and A. Relaño, Non-thermal excited-state quantum phase transitions, Europhys. Lett. **104**, 50007 (2013).
[20] B. Dietz, F. Iachello, M. Miski-Oglu, N. Pietralla, A. Richter, L. von Smekal, and J. Wambach, Lifshitz and excited-state quantum phase transitions in microwave Dirac billiards, Phys. Rev. B **88**, 104101 (2013).
[21] N. F. Zobov, S. V. Shirin, O. L. Polyansky, J. Tennyson, P.-F. Coheur, P. F. Bernath, M. Carleer, and R. Colin, Monodromy in the water molecule, Chem. Phys. Lett. **414**, 193 (2005).
[22] B. P. Winnewisser, M. Winnewisser, I. R. Medvedev, M. Behnke, F. C. De Lucia, S. C. Ross, and J. Koput, Experimental Confirmation of Quantum Monodromy: The Millimeter Wave Spectrum of Cyanogen Isothiocyanate NCNCS, Phys. Rev. Lett. **95**, 243002 (2005).
[23] Y. Kawaguchi and M. Ueda, Spinor BoseEinstein condensates, Phys. Rep. **520**, 253 (2012).
[24] D. M. Stamper-Kurn and M. Ueda, Spinor Bose gases: Symmetries, magnetism, and quantum dynamics, Rev. Mod. Phys. **85**, 1191 (2013).
[25] T. Zibold, E. Nicklas, C. Gross, and M. K. Oberthaler, Classical Bifurcation at the Transition from Rabi to Josephson Dynamics, Phys. Rev. Lett. **105**, 204101 (2010).

[26] W. Zhang, D. L. Zhou, M.-S. Chang, M. S. Chapman, and L. You, Coherent spin mixing dynamics in a spin-1 atomic condensate, Phys. Rev. A **72**, 013602 (2005).
[27] M.-S. Chang, Q. Qin, W. Zhang, L. You, and M. S. Chapman, Coherent spinor dynamics in a spin-1 Bose condensate, Nat. Phys. **1**, 111 (2005).
[28] L. Zhao, J. Jiang, T. Tang, M. Webb, and Y. Liu, Dynamics in spinor condensates tuned by a microwave dressing field, Phys. Rev. A **89**, 023608 (2014).
[29] Y. Liu, S. Jung, S. E. Maxwell, L. D. Turner, E. Tiesinga, and P. D. Lett, Quantum Phase Transitions and Continuous Observation of Spinor Dynamics in an Antiferromagnetic Condensate, Phys. Rev. Lett. **102**, 125301 (2009).
[30] E. M. Bookjans, A. Vinit, and C. Raman, Quantum Phase Transition in an Antiferromagnetic Spinor Bose-Einstein Condensate, Phys. Rev. Lett. **107**, 195306 (2011).
[31] Z. Zhang and L.-M. Duan, Generation of Massive Entanglement through an Adiabatic Quantum Phase Transition in a Spinor Condensate, Phys. Rev. Lett. **111**, 180401 (2013).
[32] X.-Y. Luo, Y.-Q. Zou, L.-N. Wu, Q. Liu, M.-F. Han, M. K. Tey, and L. You, Deterministic entanglement generation from driving through quantum phase transitions, Science **355**, 620 (2017).
[33] T. Tian, H.-X. Yang, L.-Y. Qiu, H.-Y. Liang, Y.-B. Yang, Y. Xu, and L.-M. Duan, Observation of Dynamical Quantum Phase Transitions with Correspondence in an Excited State Phase Diagram, Phys. Rev. Lett. **124**, 043001 (2020).
[34] C. B. Dağ, Sheng-Tao Wang, and L.-M. Duan, Classification of quench-dynamical behaviors in spinor condensates, Phys. Rev. A **97**, 023603 (2018).
[35] L. Pezzè, M. Gessner, P. Feldmann, C. Klempt, L. Santos, and A. Smerzi, Heralded Generation of Macroscopic Superposition States in a Spinor Bose-Einstein Condensate, Phys. Rev. Lett. **123**, 260403 (2019).
[36] T. M. Hoang, H. M. Bharath, M. J. Boguslawski, M. Anquez, B. A. Robbins, and M. S. Chapman, Adiabatic quenches and characterization of amplitude excitations in a continuous quantum phase transition, Proc. Natl. Acad. Sci. U.S.A. **113**, 9475 (2016).
[37] Y.-Q. Zou, L.-N. Wu, Q. Liu, X.-Y. Luo, S.-F. Guo, J.-H. Cao, M. K. Tey, and L. You, Beating the classical precision limit with spin-1 Dicke states of more than 10,000 atoms, Proc. Natl. Acad. Sci. U.S.A. **115**, 6381 (2018).
[38] G. A. Raggio and R. F. Werner, Quantum statistical mechanics of general mean field systems, Helv. Phys. Acta **62**, 980 (1989).
[39] N. G. Duffield and R. F. Werner, Mean-field dynamical semigroups on C^*-algebras, Rev. Math. Phys. **04**, 383 (1992).
[40] N. G. Duffield and R. F. Werner, Classical Hamiltonian dynamics for quantum Hamiltonian mean-field limits, in *Stochastics and Quantum Mechanics, Proceedings of a Conference held in Swansea, UK, 1986*, edited by A. Truman and I. M. Davies (World Scientific Publishing, Singapore, 1992), pp. 115–129, https://dx.doi.org/10.1142/9789814537452.
[41] See Supplemental Material, which includes Refs. [42–45], at http://link.aps.org/supplemental/10.1103/PhysRevLett.126.230602 for details on the mean-field limit of bosonic systems in general and of ferromagnetic spin-1 BECs in particular.
[42] P. Loya, *Amazing and Aesthetic Aspects of Analysis* (Springer, New York, NY, 2017), https://dx.doi.org/10.1007/978-1-4939-6795-7.
[43] K. Königsberger, *Analysis*, 5th ed. (Springer, Berlin, Heidelberg, 2004), Vol. 2, https://dx.doi.org/10.1007/3-540-35077-2.
[44] O. Forster, *Analysis*, 11th ed. (Springer Spektrum, Wiesbaden, 2013), Vol. 1, https://dx.doi.org/10.1007/978-3-658-00317-3.
[45] P. Feldmann, M. Gessner, M. Gabbrielli, C. Klempt, L. Santos, L. Pezzè, and A. Smerzi, Interferometric sensitivity and entanglement by scanning through quantum phase transitions in spinor Bose-Einstein condensates, Phys. Rev. A **97**, 032339 (2018).
[46] P. Stránský and P. Cejnar, Classification of excited-state quantum phase transitions for arbitrary number of degrees of freedom, Phys. Lett. A **380**, 2637 (2016).
[47] P. Ribeiro, J. Vidal, and R. Mosseri, Exact spectrum of the Lipkin-Meshkov-Glick model in the thermodynamic limit and finite-size corrections, Phys. Rev. E **78**, 021106 (2008).
[48] B. Lücke, M. Scherer, J. Kruse, L. Pezzé, F. Deuretzbacher, P. Hyllus, O. Topic, J. Peise, W. Ertmer, J. Arlt, L. Santos, A. Smerzi, and C. Klempt, Twin matter waves for interferometry beyond the classical limit, Science **334**, 773 (2011).
[49] I. Kruse, K. Lange, J. Peise, B. Lücke, L. Pezzè, J. Arlt, W. Ertmer, C. Lisdat, L. Santos, A. Smerzi, and C. Klempt, Improvement of an Atomic Clock Using Squeezed Vacuum, Phys. Rev. Lett. **117**, 143004 (2016).
[50] D. A. Steck, Quantum and atom optics, available online at http://steck.us/teaching (revision 0.13.4, 2020).